Special Feature: Dynamics Modeling Supporting Vehicle Performance

Research Report

Experimental Analysis of Driver Motion and Applied Forces Using the Instantaneous Screw Axis and the Line of Action of the Applied Forces

Takahiro Yamaguchi and Masatoshi Hada

Report received on Aug. 28, 2016

ABSTRACT A driver uses his/her muscles to apply forces and torques to the steering wheel and, in turn, receive reaction forces and torques from the steering wheel, which are in part countered by the shoulder support of the seatback. Therefore, shoulder support is considered to affect the driver's ease-of-steering feeling. The three-dimensional motion of a rigid body can be described as a rotation about a fixed axis. Similarly, the force and torque applied to a rigid body can be regarded as a force along a line of action. Thus, the present study experimentally examines the effect of the shoulder support of the seatback on the ease-of-steering feeling by investigating the equilibrium of forces and torques around the driver's shoulder girdle and arms in terms of the instantaneous axis of the driver's motion and the line of action of the forces and torques applied by the driver. During virtual slalom maneuvering on a six-axis motion base, driver's motions, forces, and torques applied to a steering wheel and seatback were measured for four scapula support modes. The lines of action of these forces and the glenohumeral joint torque about the axis parallel to steering rotation axis were then estimated. The results indicate that, during turning, the seatback reaction force is continuously applied to the medial border of the driver's moving scapula on the outer side of the turn, thereby reducing glenohumeral joint torques required for steering wheel rotation, which may enhance the ease-of-steering feeling.

KEYWORDS Human Engineering, Biomechanics, Operability, Ease-of-steering Feeling, Shoulder, Seat

1. Introduction

When steering a vehicle, the driver uses muscles to generate torques about their joints and to exert forces on the steering wheel via his/her hands to rotate the steering wheel. At the same time, a reaction force from the steering wheel acting on his/her hands is transmitted through his/her hands, arms, and shoulders to the seatback. Moreover, the level of the driver's muscular activity to maintain his/her posture against inertial forces varies with the properties of the seat.[1] Therefore, the properties of the seatback are thought to have some effect on the driver's ease-of-steering feeling.

The relation between the steering wheel pushing force and the mechanical characteristics of the seat-driver-steering system was investigated experimentally based on steering wheel disturbance torque applying experiments and system identification.[2] This study shows that pushing on the steering wheel increases the stiffness of the system mainly due to increased muscle stiffness. Moreover, we show that shoulder support of the seatback can make it easier for drivers to maintain their posture against the reaction force due to pushing against the steering wheel. Tomiyama et al. investigated how the properties of seats effect driver motion and body pressure distribution in experiments with an actual vehicle.[3] They showed that seats that hold drivers sufficiently reduce the displacement of the driver's waist, chest, and head by supporting the upper body, including the scapula. In addition, we previously investigated the relation between driver motion and internal torques experimentally using a steering reaction force simulator and found that the scapula rotates externally around the yaw axis even during very small steering maneuvers.[4] Moreover, the internal torque about the lumbosacral joint varies depending on the scapula support condition of the seat. All of these findings indicate that a seatback that effectively supports the driver's scapulae can enhance the driver's ease-of-steering feeling. However, the specific

properties of the seatback that provide sufficient scapula support remain unknown.

Therefore, in order to find out the properties of the seatback to enhance the ease-of-steering feeling, the regions of the driver's body that receive forces and torques from the steering wheel and the seatback during steering should be investigated in detail. However, since measured forces and torques are commonly analyzed separately, computing the application point of these forces and torques experimentally is difficult. Moreover, the equilibrium of forces and torques around the driver's shoulder girdle and arms during steering should be considered in order to clarify the driver's workload from the ease-of-steering aspect. Inverse dynamics analysis is a common technique for analyzing the equilibrium of forces and torques, whereas experimentally measuring all external forces and torques and computing all of the joint angles of the driver for inverse dynamics analysis is difficult.

In the analysis of human behavior, analyses of motions are commonly performed separately for the translation and rotation of the human body, and analyses of forces and torques are also commonly performed separately for forces and torques. However, it is difficult for us to understand the relation among motions, forces, and the human body by visualizing them with two different indexes, e.g., translation and rotation for human motions. Moreover, in the field of classical mechanics, the three-dimensional motion of a rigid body can be described as a rotation about a fixed axis. Also, the force and torque applied to a rigid body can be regarded as a force along a line. Therefore, we use the instantaneous screw axis to visualize the translation and rotation of the driver's body with a unified index and the line of action to visualize the forces and torques applied by the driver. Moreover, in the present study, we use these visualization tools to investigate the relation between the scapula support mode and the ease-of-steering feeling based on the equilibrium of forces and torques around driver's shoulder girdle and arms. In particular, we analyze the application points of the seat support force of the seatback to the driver's scapula. We believe that, in order to investigate the effect of the force on the driver, analyzing the application points of the seat support force on the scapula is better than analyzing the application points on the seatback.

2. Instantaneous Screw Axis and Line of Action

2. 1 Velocity, Angular Velocity, and Instantaneous Screw Axis

Let us begin by considering the three-dimensional motion of rigid body B, as shown in **Fig. 1**(a). The position of an arbitrary point, P, on rigid body B, $\boldsymbol{x}_p \in \Re^3$, can be described as

$$\boldsymbol{x}_p = \boldsymbol{x}_o + \boldsymbol{A}\boldsymbol{s}', \tag{1}$$

where $\boldsymbol{x}_o \in \Re^3$ is the origin of the coordinate frame $\Sigma_{x'y'z'}$, which moves along with rigid body B; $\boldsymbol{A} \in \Re^{3\times3}$ is the direction cosine matrix from $\Sigma_{x'y'z'}$ to Σ_{xyz}, and $\boldsymbol{s}' \in \Re^3$ is the position of P described in $\Sigma_{x'y'z'}$. Differentiating Eq. (1) with respect to time and using $\boldsymbol{A}^{-1} = \boldsymbol{A}^T$ yields the velocity of point P, $\boldsymbol{v}_p \in \Re^3$, as follows:

$$\boldsymbol{v}_p = \dot{\boldsymbol{x}}_o + \dot{\boldsymbol{A}}\boldsymbol{s}', \tag{2}$$

$$\boldsymbol{s}' = \boldsymbol{A}^T(\boldsymbol{x}_p - \boldsymbol{x}_o). \tag{3}$$

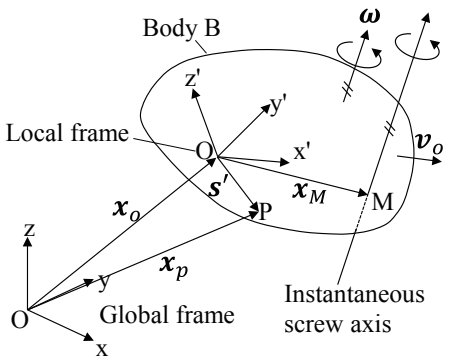

(a) Translation and rotation regarding rigid body B

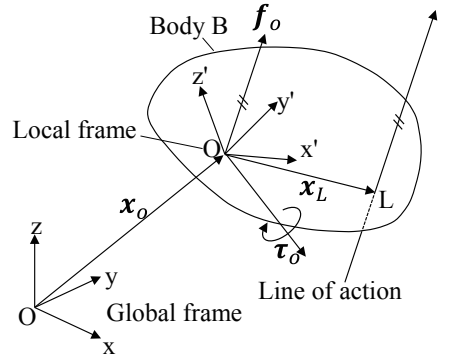

(b) Force and torque applied on x_o on rigid body B

Fig. 1 Motion and force of a rigid body.

The angular velocity of rigid body B in Σ_{xyz} is defined as $\boldsymbol{\omega} = [\omega_x \quad \omega_y \quad \omega_z]^T \in \Re^3$. Then, substituting Eq. (3) for Eq. (2) with the Poisson equation yields

$$\boldsymbol{v}_p = \dot{\boldsymbol{x}}_o + \dot{\boldsymbol{A}}\boldsymbol{A}^T(\boldsymbol{x}_p - \boldsymbol{x}_o), \tag{4}$$

$$\boldsymbol{v}_p = \boldsymbol{v}_o + \tilde{\boldsymbol{\omega}}(\boldsymbol{x}_p - \boldsymbol{x}_o), \tag{5}$$

$$\tilde{\boldsymbol{\omega}} = \begin{bmatrix} 0 & -\omega_z & \omega_y \\ \omega_z & 0 & -\omega_x \\ -\omega_y & \omega_x & 0 \end{bmatrix}, \tag{6}$$

where $\boldsymbol{v}_o \in \Re^3$ is the velocity of point $\boldsymbol{x}_o$, and $\sim$ indicates a skew symmetric operation.[5] The point M on rigid body B that has the minimum velocity and the minimum distance from $\boldsymbol{x}_o$ can be obtained as

$$\boldsymbol{x}_M = \frac{\tilde{\boldsymbol{\omega}}}{|\boldsymbol{\omega}|^2}\boldsymbol{v}_o + \left(\boldsymbol{I} - \frac{\boldsymbol{\omega}\boldsymbol{\omega}^T}{|\boldsymbol{\omega}|^2}\right)\boldsymbol{x}_o, \tag{7}$$

where $\boldsymbol{I} \in \Re^{3\times3}$ is the unit matrix.[6] Using Eqs. (5) and (7), $\boldsymbol{v}_p$ can be redefined as

$$\boldsymbol{v}_p = \boldsymbol{u}\frac{\boldsymbol{\omega}}{|\boldsymbol{\omega}|} + \tilde{\boldsymbol{\omega}}(\boldsymbol{x}_p - \boldsymbol{x}_M), \tag{8}$$

$$\boldsymbol{u} = \frac{1}{|\boldsymbol{\omega}|}\boldsymbol{\omega}^T\boldsymbol{v}_o. \tag{9}$$

The instantaneous screw axis can be defined based on $\boldsymbol{v}_o$ and $\boldsymbol{\omega}$ as an axis along $\boldsymbol{\omega}$ passing through point $\boldsymbol{x}_M$. The first term of Eq. (8) is the velocity component of an arbitrary point on the rigid body along the instantaneous screw axis, and the second term is the component about the same axis.

2. 2 Force, Torque, and Line of Action

Next, consider a force $\boldsymbol{f}_o \in \Re^3$ exerted on point $\boldsymbol{x}_o$ on rigid body B and a torque $\boldsymbol{\tau}_o \in \Re^3$ about point $\boldsymbol{x}_o$, as shown in Fig. 1(b). Then, the torque $\boldsymbol{\tau}_p \in \Re^3$ about an arbitrary point $\boldsymbol{x}_p$ on rigid body B can be described as follows:

$$\boldsymbol{\tau}_p = \boldsymbol{\tau}_o + \widetilde{(\boldsymbol{x}_o - \boldsymbol{x}_p)}\boldsymbol{f}_o, \tag{10}$$

$$\boldsymbol{\tau}_p = \boldsymbol{\tau}_o + \tilde{\boldsymbol{f}}_o(\boldsymbol{x}_p - \boldsymbol{x}_o). \tag{11}$$

Let us assume that point $\boldsymbol{x}_L \in \Re^3$ on the rigid body has the minimum torque. Similarly, based on the calculations of the previous section, the following equations are obtained in terms of $\boldsymbol{x}_p$ on rigid body B:

$$\boldsymbol{\tau}_p = \boldsymbol{m}\frac{\boldsymbol{f}_o}{|\boldsymbol{f}_o|} + \tilde{\boldsymbol{f}}_o(\boldsymbol{x}_p - \boldsymbol{x}_L), \tag{12}$$

$$\boldsymbol{m} = \frac{1}{|\boldsymbol{f}_o|}\boldsymbol{f}_o{}^T\boldsymbol{\tau}_o, \tag{13}$$

$$\boldsymbol{x}_L = \frac{\tilde{\boldsymbol{f}}_o}{|\boldsymbol{f}_o|^2}\boldsymbol{\tau}_o + \left(\boldsymbol{I} - \frac{\boldsymbol{f}_o\boldsymbol{f}_o{}^T}{|\boldsymbol{f}_o|^2}\right)\boldsymbol{x}_o. \tag{14}$$

Based on Eqs. (12) to (14), the situation thus far is equivalent to a force $\boldsymbol{f}_o$ applied at $\boldsymbol{x}_L$ concurrently with a torque $\boldsymbol{m}$ applied about $\boldsymbol{x}_L$. The line of action can be described as the line along $\boldsymbol{f}_o$, which passes through $\boldsymbol{x}_L$.

2. 3 Visualization of the Instantaneous Screw Axis and the Line of Action

When analyzing a driver's body motion using the instantaneous screw axis or the force and torque applied by a driver using the line of action, two points are of critical importance: (i) the point at which the screw axis or the line of action of rigid body B passes through rigid body B, and (ii) the point at which the screw axis or the line of action of rigid body B passes through rigid body C (any other rigid body). The relative position of $\boldsymbol{x}_M$ or $\boldsymbol{x}_L$ with respect to $\boldsymbol{x}_o$ can be used in evaluating (i). For instance, **Fig. 2** shows the instantaneous screw axis the center of mass of the pelvis, with a line through $\boldsymbol{x}_M$, scaled according to the magnitude of $\boldsymbol{\omega}$ when the pelvis is translated laterally and rotated around the yaw and roll axes.

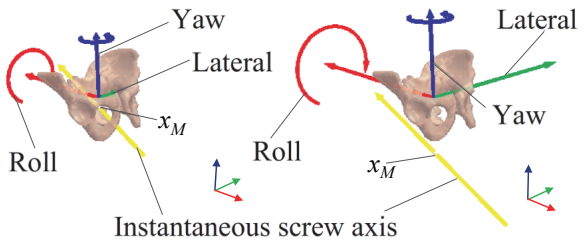

(a) Small lateral velocity ($\boldsymbol{v}_\perp$) case (b) Large lateral velocity ($\boldsymbol{v}_\perp$) case

Fig. 2 Example of instantaneous screw axis.

The components of $\boldsymbol{v}$ can be divided into components orthogonal to and parallel to $\boldsymbol{\omega}$, i.e., $\boldsymbol{v}_{\perp}$, and $\boldsymbol{v}_{//}$. When $\boldsymbol{v}_{\perp}$ is smaller, the axis is closer to the pelvis, and when $\boldsymbol{v}_{\perp}$ is larger, the axis is further from the pelvis. When analyzing (ii), it is necessary to obtain $\boldsymbol{x}_N \in \Re^3$. By calculating the intersection point between the screw axis, or the line of action, and the plane that has normal vector $\boldsymbol{n} \in \Re^3$ and contains a point on rigid body C, as shown in **Fig. 3**, we obtain the following:

$$\boldsymbol{x}_N = \boldsymbol{x}_M + \frac{\boldsymbol{n}^T(\boldsymbol{x}_o - \boldsymbol{x}_M)}{\boldsymbol{n}^T\boldsymbol{\omega}}\boldsymbol{\omega}\,,$$

$$\boldsymbol{x}_N = \boldsymbol{x}_L + \frac{\boldsymbol{n}^T(\boldsymbol{x}_o - \boldsymbol{x}_L)}{\boldsymbol{n}^T\boldsymbol{f}_o}\boldsymbol{f}_o\,. \tag{15}$$

Moreover, $\boldsymbol{x}_N$ can be defined as the foot of a perpendicular from $\boldsymbol{x}_o$ to the axis or line of action, as follows:

$$\boldsymbol{x}_N = \boldsymbol{x}_M + \frac{\boldsymbol{\omega}^T(\boldsymbol{x}_o - \boldsymbol{x}_M)}{\boldsymbol{\omega}^T\boldsymbol{\omega}}\boldsymbol{\omega}\,,$$

$$\boldsymbol{x}_N = \boldsymbol{x}_L + \frac{\boldsymbol{f}_o{}^T(\boldsymbol{x}_o - \boldsymbol{x}_L)}{\boldsymbol{f}_o{}^T\boldsymbol{f}_o}\boldsymbol{f}_o\,. \tag{16}$$

3. Experiments

3. 1 Apparatus

As shown in **Fig. 4**, the experimental apparatus essentially consists of a six-axis motion base, an image projection system, a steering reaction force simulator, a steering force/torque sensor, a capacitive pressure distribution sensor, a motion capture system, and a test seat.

The six-axis motion base includes three pairs of pantographic parallel-linked arms, each driven by an AC servomotor, which control the pedestal position and attitude.

The image projection system projects the driving scene and indicates the target steering angle as well as the actual steering angle onto a screen in front of the driver. The driver maneuvers the steering wheel by adjusting the actual steering angle to match the target steering angle.

The steering reaction force simulator computes the target steering reaction force from a linear bicycle model based on the lateral force of the tires and outputs the computed reaction force or torque.

The steering force/torque sensor is a steering wheel with two six-axis force/torque sensors (Mini; ATI Industrial Automation, Inc.) mounted on the left and right spokes. The forces and torques (hereinafter, referred to simply as the steering force) applied by the driver to the left and right sides of the steering wheel can be measured independently.

The capacitive pressure distribution sensor (LX200; Xsensor Technology Corp.) was mounted to the test seatback and was used to measure changes in the body pressure distribution.

The motion capture system (MX-T Camera System; Vicon Motion Systems Ltd.), comprising motion capture cameras and optical markers attached to the experimental subjects and apparatus, was used to capture the motions of the driver and the experimental apparatus.

3. 2 Test Seat and Scapula Support Mode

As shown schematically in **Fig. 5**, the seatback of

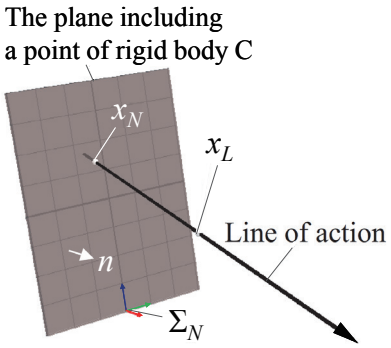

Fig. 3 Example of line of action.

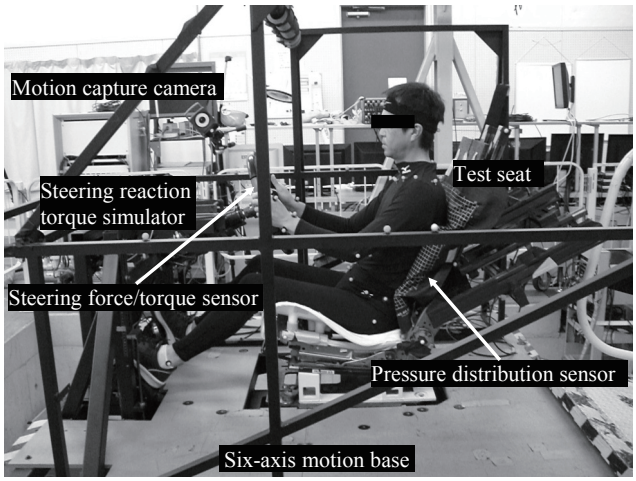

Fig. 4 Experimental system overview.

the test seat is segmented into trunk, left-shoulder, and right-shoulder support segments. The surfaces of the shoulder-support segments are rigid flat plates that can be adjusted depending on the support mode by changing the attached scapula support components. The forces and torques applied to the driver's left- and right-shoulder support segments (hereinafter, referred to simply as the seat support force) are measured separately using six-axis force/torque sensors (Delta; ATI Industrial Automation, Inc.) attached behind the left and right plates.

As shown schematically in **Fig. 6**, the following four modes of contact between the seatback and the scapulae were used to investigate the relation between the scapula support mode and ease-of-steering feeling: A) contact mainly with the medial border of the scapula, B) contact mainly with the inferior-angle of the scapula, C) contact mainly with the lateral border of the scapula, and D) contact with a large area in the superior region extending from the lateral border of the scapula. The shapes of the scapula support components for each scapula support mode were designed for a driver holding the steering wheel at a neutral angle, i.e., 0 degrees.

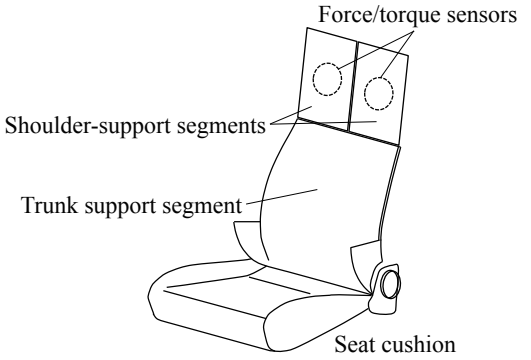

Fig. 5 Test seat overview.

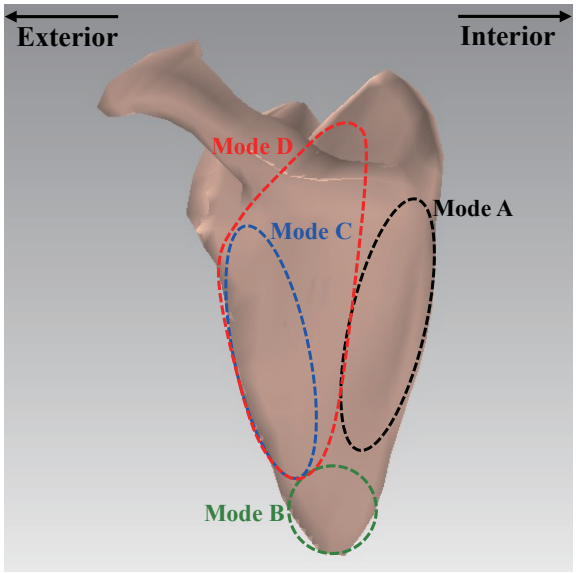

Fig. 6 Seatback contact area of left scapula.

3. 3 Target Steering Angle and Six-axis Motion Base Movement

In the experiments, the target steering angle was indicated by the image projector in order to control the subject's steering. As shown in **Fig. 7** (left), the target steering angle was set to follow a slalom course in which the steering wheel was held at the neutral angle for a short time. Specifically, the target steering angle followed a sinusoidal arc with amplitude of 45 degrees and a period of 2.5 seconds, with a cutoff at 15 degrees.

The six-axis motion base moved in synchronization with the target steering angle. The lateral displacement and yaw angle of the pedestal were computed based on an equivalent linear bicycle model in terms of the target steering angle at a vehicle speed of 100 km/h, as shown in Fig. 7 (right). Moreover, the roll angle of the platform was calculated by assuming the roll angle to be a delayed secondary response to the vehicle lateral acceleration. The analysis period was taken as a period during which a stable steering state was presumably achieved by the driver, as shown in Fig. 7.

3. 4 Procedure

The experiments to understand the relation between the scapula support mode and the ease-of-steering

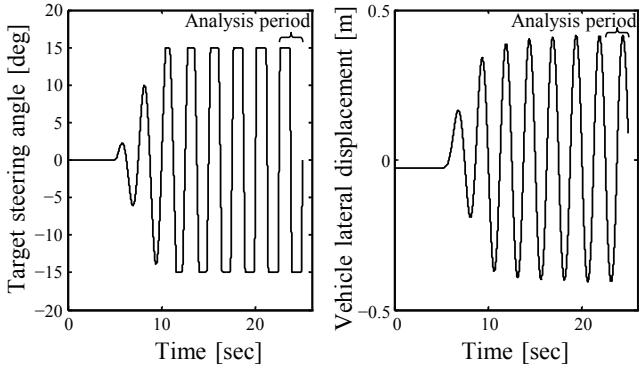

Fig. 7 Target steering angle and vehicle lateral motion.

feeling were performed with one skilled male test driver (height: 170 cm, weight: 60 kg). The assessment was approved internally, and the informed consent of the driver was obtained in advance following a full detailed explanation. The subject was seated in the test seat mounted on the pedestal of the six-axis motion base and performed the simulated slalom driving including periods during which the steering wheel was held at a fixed angle for a time. The subject was instructed to match the actual steering angle to the target steering angle shown by the image projector and reported his sensory assessment of the ease-of-steering feeling for each of the modes of contact with the scapula.

4. Analytical Method

4. 1 Estimation of Scapula Movement

It is well known that the scapulae slide over the thorax, and the relation between the scapulae and the thorax is considered to be a functional joint, known as the scapulothoracic joint. Accurate estimation of scapula movement was required for clarification of the relation between the scapula support mode and the ease-of-steering feeling. However, scapulae movement cannot be estimated directly by the motion capture system alone, because the scapulae inherently undergo substantial movement relative to the skin, and a large portion of the scapular region was blocked from view by the seatback.

We therefore approximated the thorax as an ellipsoid and added a constraint condition in which the velocity, $\boldsymbol{v}$, of a constraint point on the inferior angle relative to the ellipsoid and a vector, $\boldsymbol{n}$, normal to the ellipsoid are orthogonal to each other. The equation of constraint is then

$$C(\boldsymbol{n},\boldsymbol{v}) = \boldsymbol{n}^T \cdot \boldsymbol{v} = \left(\boldsymbol{n}^T \cdot \boldsymbol{J}(\boldsymbol{q}(t))\right) \cdot \dot{\boldsymbol{q}}(t) \equiv \boldsymbol{C}_q(\boldsymbol{q}(t)) \cdot \dot{\boldsymbol{q}}(t) = 0, \quad (17)$$

where $\boldsymbol{q}(t)$ is the body joint displacement and $\boldsymbol{J}(\boldsymbol{q}(t))$ is the Jacobian matrix related to the position of the constraint point $\boldsymbol{q}(t)$. We combined this constraint with the movement of the two optical markers attached in the region of the upper scapulae and performed inverse kinematic computation, to estimate the scapular movement (**Fig. 8**).

4. 2 Inertia Compensation for Steering Force and Seat Support Force

In order to analyze the forces and torques applied by drivers on the moving motion base or vehicles, the inertia forces and torques exerted on the strain body of the six-axis force/torque sensors cannot be ignored, and so we compensate the inertia forces and torques using the following techniques. For this purpose, we denote the reference coordinate system as Σ_0, the six-axis motion base coordinate system as Σ_m, and the coordinate system of the center of mass of the strain body as Σ_c. Then, if we denote the homogeneous transformation matrix that transforms Σ_m into Σ_0 as ${}^0\boldsymbol{T}_m \in \Re^{4\times4}$ and the homogeneous transformation matrix transforms Σ_c into Σ_m as $\boldsymbol{E}_c \in \Re^{4\times4}$, then the homogeneous transformation ${}^0\boldsymbol{T}_c \in \Re^{4\times4}$ that transforms Σ_c into Σ_0 can be represented as

$${}^0\boldsymbol{T}_c = {}^0\boldsymbol{T}_m\boldsymbol{E}_c\,. \quad (18)$$

If we now take the six-axis force/torque sensor and its strain body to be fixed relative to the pedestal of six-axis motion base, then the acceleration of Σ_c can be represented in Σ_0 as

$${}^0\ddot{\boldsymbol{T}}_c = {}^0\ddot{\boldsymbol{T}}_m\boldsymbol{E}_c\,. \quad (19)$$

Similarly, if we denote the sensor origin coordinate system as Σ_s and the homogeneous transformation matrix transforming Σ_s into Σ_m as $\boldsymbol{E}_s \in \Re^{4\times4}$, then the homogeneous transformation matrix ${}^0\boldsymbol{T}_s \in \Re^{4\times4}$ that transforms Σ_s into Σ_0 can be represented as

$${}^0\boldsymbol{T}_s = {}^0\boldsymbol{T}_m\boldsymbol{E}_s, \quad (20)$$

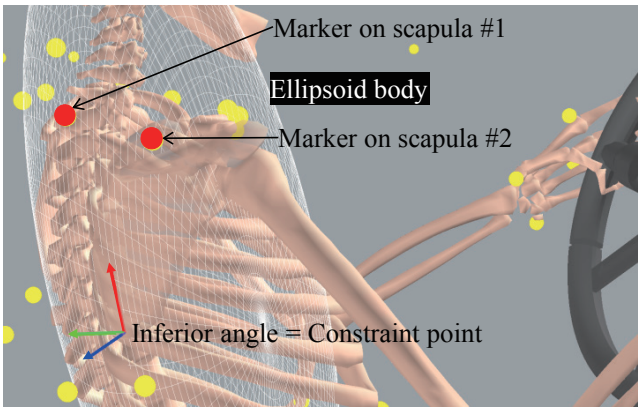

Fig. 8 Estimation method of scapula motion.

and accordingly the acceleration ${}^{s}\ddot{\boldsymbol{T}}_c \in \Re^{4\times4}$ of Σ_c in Σ_s can be obtained as

$$ {}^{s}\ddot{\boldsymbol{T}}_c = {}^{0}\boldsymbol{T}_s^{-1} \cdot {}^{0}\ddot{\boldsymbol{T}}_c. \tag{21} $$

By defining the coordinates of Σ_c in Σ_s as

$$ \boldsymbol{x}_c = [x_c \quad y_c \quad z_c]^T, \tag{22} $$

we obtain the inertia force $\boldsymbol{F}_i \in \Re^3$ elements as

$$ \begin{aligned} \boldsymbol{F}_i &= \left[F_x^i \quad F_y^i \quad F_z^i\right]^T \\ &= \left[-M\,{}^{s}\ddot{\boldsymbol{T}}_c^{(1,4)} \quad -M\,{}^{s}\ddot{\boldsymbol{T}}_c^{(2,4)} \quad -M\,{}^{s}\ddot{\boldsymbol{T}}_c^{(3,4)}\right], \end{aligned} \tag{23} $$

where M is the mass of the strain body, and ${}^{s}\ddot{\boldsymbol{T}}_c^{(j,k)}$ is the element in row j and column k of the matrix ${}^{s}\ddot{\boldsymbol{T}}_c$. We also obtain the $\boldsymbol{\tau}_i$ elements as

$$ \boldsymbol{\tau}_i = \left[F_z^i y_c - F_y^i z_c \quad F_x^i z_c - F_z^i x_c \quad F_y^i x_c - F_x^i y_c\right]^T, \tag{24} $$

which we then divide by the measured force $\boldsymbol{F}_m \in \Re^3$ and the measured torque $\boldsymbol{\tau}_m \in \Re^3$, respectively, thus performing the inertial force compensation.

4. 3 Estimation of the Application Point of the Seat Support Force

Following the inertia compensation, we next determined the region of the scapula to which seat support forces were applied by computing the application points of these forces on the scapula with after-mentioned techniques. Moreover, we also obtained the region of the seatback to which these forces applied.

First, we defined the planes S_{LS} and S_{RS} fixed to the moving left and right scapulae and the plane S_B fixed to the seatback. These planes were fixed as nearly as possible to the region targeted for the computation of the application points of the forces. Secondly, regarding the left shoulder girdle and arm, we obtained the intersection of the line of action of the left shoulder support force, $\boldsymbol{F}_{LS}$, and S_{LS} as application point P_{LS}. Similarly, we determined the application point, P_{RS}, of the right shoulder support force, $\boldsymbol{F}_{RS}$, on the right scapula. Then, the application point P_{LB} of $\boldsymbol{F}_{LS}$ on the seatback was obtained as the intersection of the line of action of $\boldsymbol{F}_{LS}$ and S_B. Moreover, P_{RB} of $\boldsymbol{F}_{RS}$ on the seatback was also obtained (**Fig. 9**).

4. 4 Ratio of Steering Torque Support by the Seat

If drivers can maneuver the steering wheel with only small joint torque exerted by activating their muscles, they report steering as being relatively easy. Thus, we estimated the glenohumeral joint torque generated by the driver while holding the steering wheel based on the measured steering and seat support forces. The equation of motion of the driver's shoulder girdle and arms about the glenohumeral joint while holding the steering wheel is expressed as

$$ \boldsymbol{M}(\boldsymbol{q})\ddot{\boldsymbol{q}} + \boldsymbol{C}(\boldsymbol{q},\dot{\boldsymbol{q}}) + \boldsymbol{G}(\boldsymbol{q}) = \boldsymbol{\tau} - \boldsymbol{J}(\boldsymbol{q})^T\boldsymbol{F}, \tag{25} $$

where $\boldsymbol{q}$ represents the generalized coordinates of the joint angles of driver's superior limb girdle and arms. The first term on the left-hand side of the equation represents the inertia term, and the second term represents the centrifugal and Coriolis forces. The third term represents the gravitational force and the inertia force caused by the vehicle motion. Moreover, $\boldsymbol{\tau}$ is the glenohumeral joint torque, $\boldsymbol{J}(\boldsymbol{q})$ is the Jacobian matrix about the glenohumeral joint, and $\boldsymbol{F}$ is the contact force applied by the driver.

We neglected the inertia term and the centrifugal and Coriolis force terms in Eq. (25), because the posture of the driver's superior limb girdle and arms can be assumed not to change ($\ddot{\boldsymbol{q}} = \dot{\boldsymbol{q}} = \boldsymbol{0}$) while holding the steering wheel. Moreover, the vehicle motions reproduced by the six-axis motion base are identical, and by assuming that the driver's posture is approximately the same in all four scapula support modes, we can therefore regard the gravitational term as constant. Then, the effects of the scapula support mode on the glenohumeral torque $\boldsymbol{\tau}$ can be compared in terms of $\boldsymbol{J}(\boldsymbol{q})^T\boldsymbol{F}$ alone. Based on these assumptions,

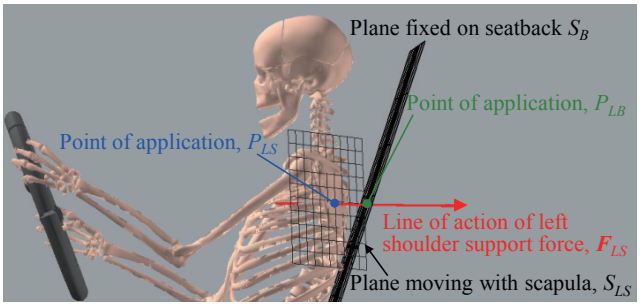

Fig. 9 Definition of point of application of seat support force on left scapula plane (P_{LS}) and seatback plane (P_{LB}).

we defined torque $\boldsymbol{\tau}_s$ as the glenohumeral torque exerted by the driver for steering after the removal of the gravitational term $\boldsymbol{G}(\boldsymbol{q})$. From Eq. (25), $\boldsymbol{\tau}_s$ is expressed as

$$\boldsymbol{\tau}_s = \boldsymbol{\tau} - \boldsymbol{G}(\boldsymbol{q}) = \boldsymbol{J}(\boldsymbol{q})^T \boldsymbol{F}. \tag{26}$$

In order to illustrate the procedure, let us consider the estimation of the torque about the left glenohumeral joint shown in **Fig. 10**. We denote the external force applied by the driver as $\boldsymbol{F}$, obtain the resultant force, $\boldsymbol{F}_{sb}$, of the steering force, $\boldsymbol{F}_s$, of the left hand and the seat support force, $\boldsymbol{F}_b$, for the left shoulder, and estimate the line of action of the resultant force as

$$\boldsymbol{F} = \boldsymbol{F}_{sb} = \boldsymbol{F}_s + \boldsymbol{F}_b. \tag{27}$$

We next find the point $\boldsymbol{x}_j$ on the line of action $\boldsymbol{F}_{sb}$ that is nearest to the glenohumeral joint and calculate the moment $\boldsymbol{\tau}_s$ about the glenohumeral joint as

$$\boldsymbol{\tau}_s = \boldsymbol{J}(\boldsymbol{q})^T \boldsymbol{F}_{sb} = \boldsymbol{x}_j \times \boldsymbol{F}_{sb}. \tag{28}$$

Finally, from the component τ_x of $\boldsymbol{\tau}_s$ that is parallel to the plane of the steering wheel rotation and the steering torque τ_{sw}, we obtain the proportion r_{sb} of τ_{sw} that is borne by the seatback (the seat support ratio) as

$$r_{sb} = \frac{\tau_{sw} - \tau_x}{\tau_{sw}} \times 100\ [\%]. \tag{29}$$

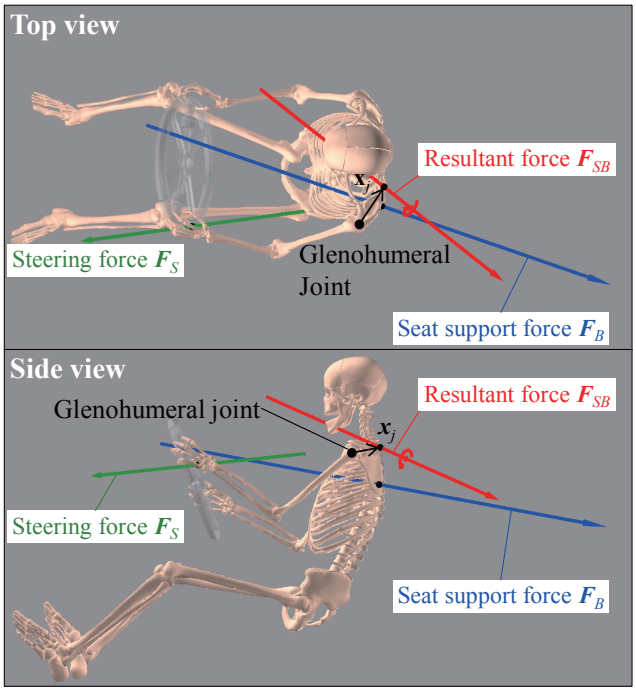

Fig. 10 A typical example of resultant force of steering force and seat support force regarding left glenohumeral joint.

5. Results and Discussions

5. 1 Sensory Assessment

The driver ranked the four modes of scapula support as D, C, B and A, in order of decreasing ease-of-steering feeling.

5. 2 Steering Angle and Steering Torque

As shown in **Fig. 11**, the overall waveforms of the steering angles and torques during the analysis period were nearly identical for all four scapula support modes, and the steering torque while holding the steering wheel was stable with very little divergence. Thus, the measured driver's motion, forces and torques were comparable in all four scapula support modes.

The period in which the steering torque rises from 0 to its maximum absolute value is called the turn period. Moreover, the period from the attainment of the maximum absolute value to the point at which 75%

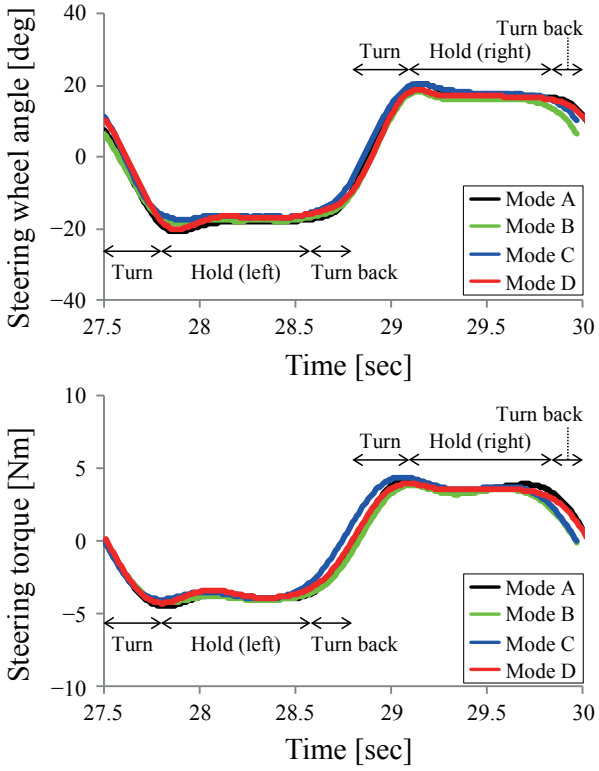

Fig. 11 Steering angle and torque during driving slalom.

of the maximum absolute value is reached is called the hold period, and that extending from 75% of the maximum absolute value to 0 is called the turn-back period. Figure 11 shows each of these three periods for mode D.

5. 3 Instantaneous Screw Axes while Turning the Steering Wheel

Figure 12 shows the instantaneous screw axis, α_t, of the thorax with respect to the floor of the six-axis motion base when the driver turned the steering wheel to the left or right at an angular velocity, ω_{sw}, of approximately 90 degrees per second. As shown in the figure, α_t became horizontally shortened for scapula support modes C and D, which earned a better rating

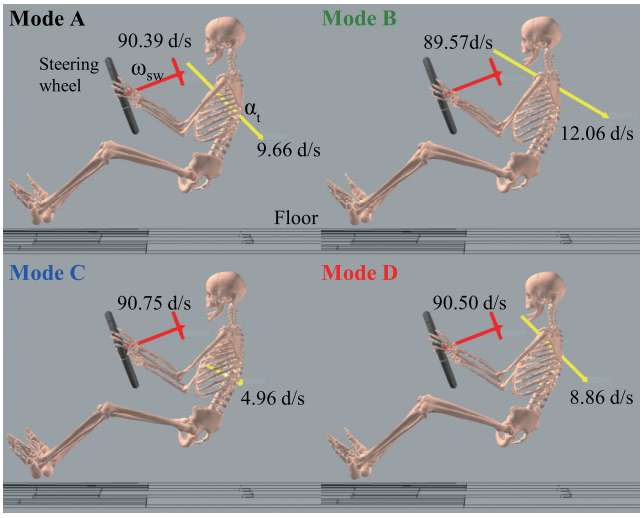

(a) During turning the steering wheel to the left

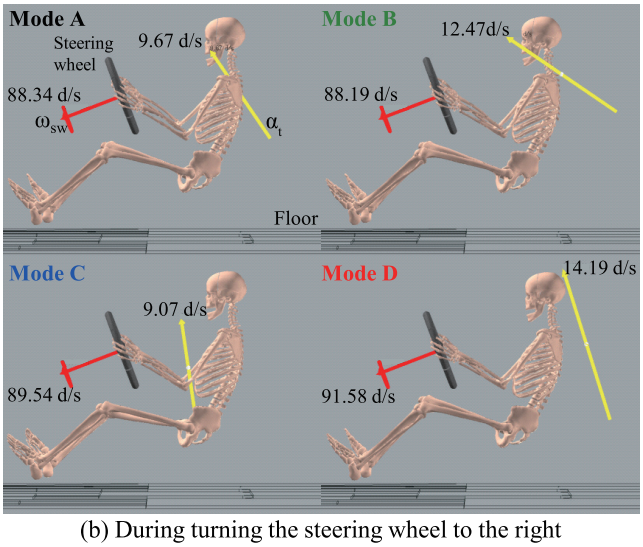

(b) During turning the steering wheel to the right

Fig. 12 Instantaneous screw axis of driver's thorax during turning the steering wheel.

from the driver. Thus, the roll rotation of the thorax driven by steering maneuvering and vehicle motion decreased for these modes. This result indicates that, in order to enhance the ease-of-steering feeling, the seat can support the driver's upper body against steering maneuvering and vehicle motion, thereby reducing the roll rotation of driver's upper body.

5. 4 Trajectory of Application Point of Seat Support Force

Figure 13 shows the trajectories of P_{LB} and P_{RB} during the analysis. In Fig. 13, the observed P_{LB} and P_{RB} trajectories for each of the four scapula support modes are superimposed on the driver's skeleton model while holding the steering wheel at the neutral angle. As shown in the figure, P_{LB} and P_{RB} moved medially in mode A, stayed near the inferior angle of the scapula in modes B and C, and, in mode D, moved through a large range from the vicinity of the inferior angle to that of the distal margin region.

Figure 14 shows the trajectories of P_{LS} and P_{RS} during the analysis period. As shown, P_{LS} and P_{RS} moved medially some distance from the scapular region in mode A, but for the other three modes, they were confined to the vicinity of the medial border of the scapula. In contrast, while holding the steering wheel, the trajectories of P_{LS} and P_{RS} were small, and, for modes A and B, were located medially from the scapula. However, for modes C and D, they were located within the scapular region, distally from its medial border.

These results clearly indicate that modes A and B were unable to support the scapula within its medial border while holding the steering wheel and maintaining the maximum steering torque. Comparison of these results with the sensory assessments made by the driver

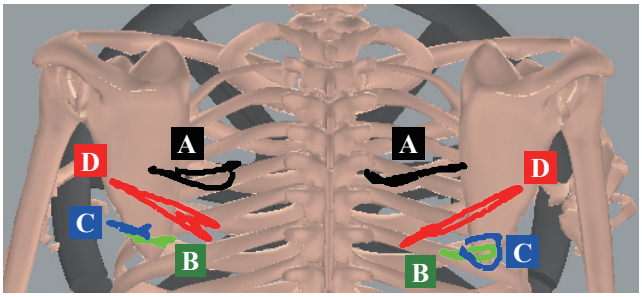

Fig. 13 Trajectories of point of application regarding seatback support force on the seatback plane.

indicates that one essential requirement for enhancing the ease-of-steering feeling is that application point of the seat support force is on medial border of the scapula, as in the cases of modes C and D.

As described in Sec. 3. 2, modes C and D are designed to support the region near lateral border of the scapula while the driver holds the steering wheel at the neutral angle (Fig. 6). In Fig. 14, however, these modes support the region near the medial border of the scapula while holding the steering wheel. This difference in the scapula support region is caused by the movement of the scapula away from the center of the turn induced by steering and vehicular acceleration.

In addition, these results were obtained by analyzing the application points of the seat support forces on the driver's moving scapulae, rather than on the seatback. Therefore, the application points on driver's moving body are thought to be valuable indexes for analyzing force application on the driver.

5. 5 Ratio of Steering Torque Borne by the Seat

Figure 15 shows the torque, τ_x, about the glenohumeral joint outside the turn when the steering torque was at its maximum absolute value for modes C and D, and **Fig. 16** shows r_{sb} at that time. The steering torque is approximately the same for both modes, but τ_x is clearly smaller in mode D, indicating a higher r_{sb} value in mode D. The glenohumeral joint torque component in the plane parallel to the plane of steering wheel rotation represents the joint torque exerted by the driver by activating his/her muscles to steer and to maintain his/her posture. Therefore, the driver is thought to steer more easily in mode D than in mode C. Moreover, assuming that the driver posture and vehicle motion were constant among the scapula support modes, scapula support mode D was found to reduce the glenohumeral joint torque by bearing a larger portion of the torque exerted for steering, as compared to mode C. Moreover, these results suggest that the lines of action of the forces exerted by the driver are good tools for estimating joint torques.

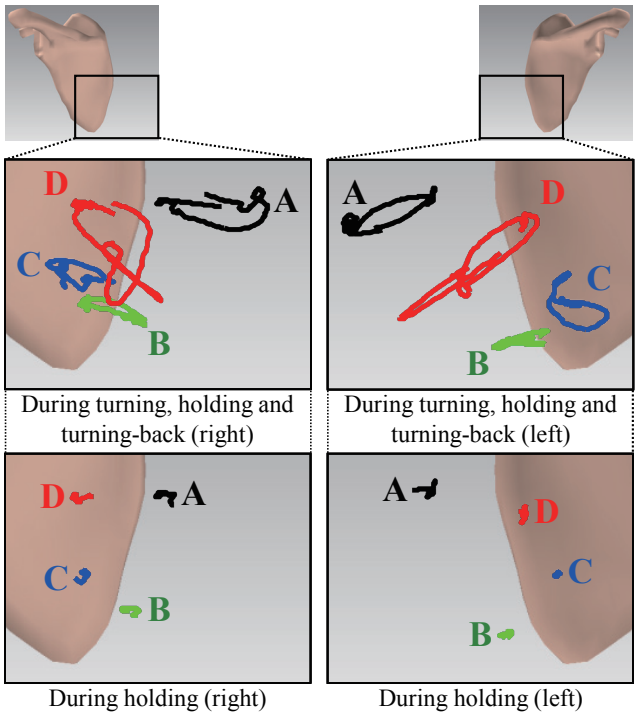

Fig. 14 Trajectory of point of application regarding seatback support force on the scapula plane.

6. Conclusions

In order to investigate supporting the driver's scapulae by the seatback and the relationship between scapula support and the ease-of-steering feeling, we focused on the forces and torques applied to the steering wheel and to the shoulder region of the seatback by the driver, as well as the equilibrium of forces and torques around the driver's shoulder girdle and arms. In particular, using a six-axis motion base, we measured the driver's motion, forces and torques during simulated driving over a slalom course that included periods during which the driver needed to hold the steering wheel at a certain angle for a period of time. Then, we investigated the relation between the driver's sensory assessment of ease of steering and the mode of scapula support. The results indicate that a seatback can enhance the driver's ease-of-steering feeling if the following two requirements are satisfied:

1) The application point of the shoulder support force by the seatback must remain over the region near the medial border of the scapulae when the scapulae move in association with the steering maneuver.

2) The seatback shoulder region must bear a substantial proportion of the forces and torques generated by the driver while steering.

The study also confirmed that it is possible to clarify the mechanisms for changing the ease-of-steering feeling of drivers by investigating the equilibrium of forces and torques around drivers based on measured motion of drivers, forces and torques exerted by

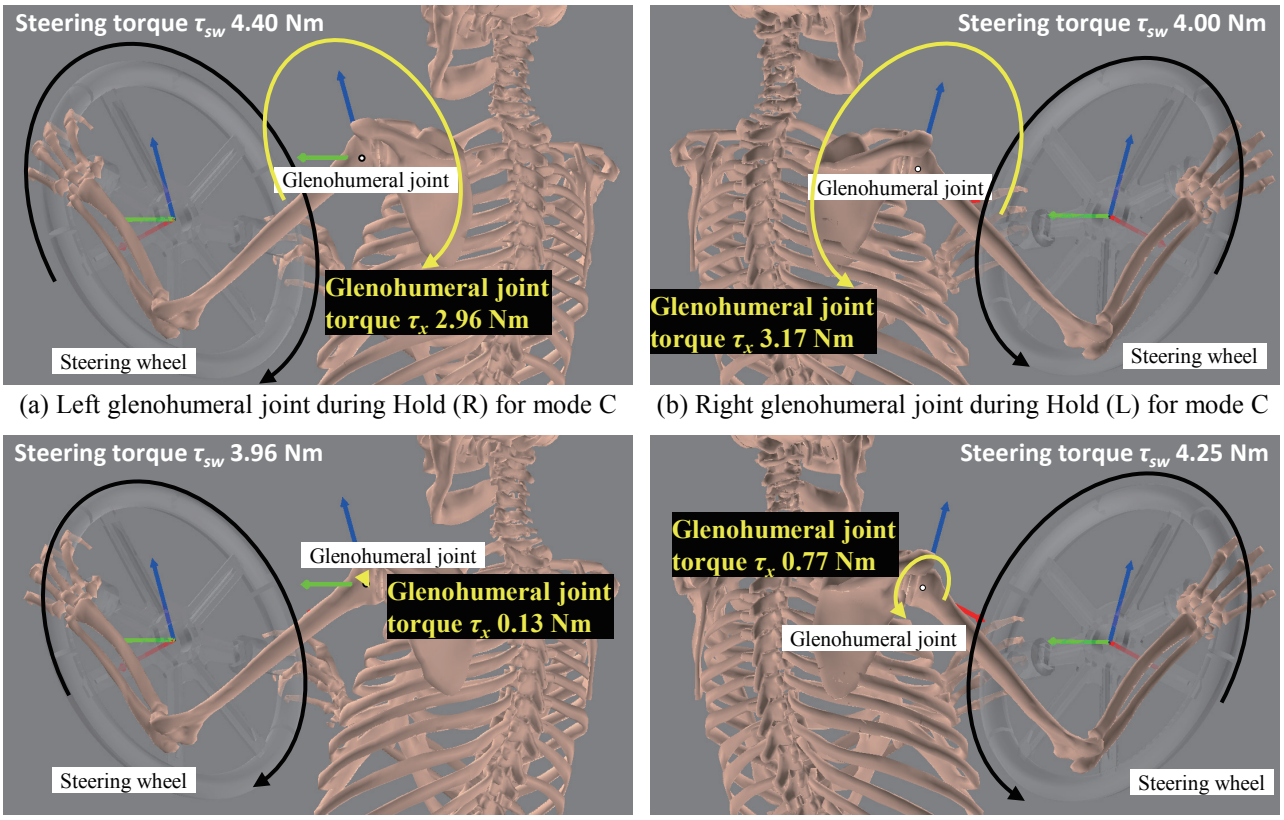

(a) Left glenohumeral joint during Hold (R) for mode C
(b) Right glenohumeral joint during Hold (L) for mode C
(c) Left glenohumeral joint during Hold (R) for mode D
(d) Right glenohumeral joint during Hold (L) for mode D

Fig. 15 Steering torque and glenohumeral joint torque when exerting maximum steering torque.

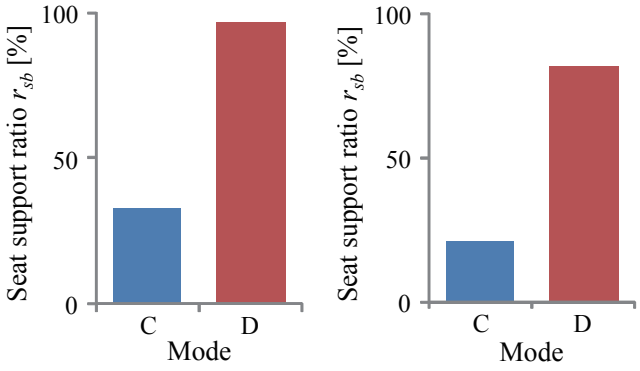

(a) During holding right
(b) During holding left

Fig. 16 Steering torque support ratio of turning outer side shoulder during holding steering wheel.

drivers. Moreover, we suggested that computing the lines of action of the forces applied by the driver or the application points of these forces on the driver's body is a valuable tool for analyzing the force application mechanism on the driver's body or the driver's physical strain.

However, our study has some limitations. In particular, only one expert driver participated in the experiment, and further testing is needed in order to determine whether the findings are widely applicable. Comparison of the seatback area was only performed for the shoulder support, but other regions of the seat, such as the lumber support, side support, and seat cushion, should also be investigated. The maximum steering wheel angle was approximately 15 degrees, and the vehicle lateral acceleration was up to approximately 0.2 G. However, a wider variety of driving environments should be investigated in the future.

Finally, we assumed that the posture of the driver's shoulder girdle and arms did not change while holding the steering wheel when we estimated the glenohumeral joint torque. However, this assumption does not hold for situations in which drivers are rotating the steering wheel or in which their bodies are subjected to higher vehicle accelerations. Therefore, inverse dynamics analysis of driver's motions, forces and torques is necessary in order to analyze these situations. We are

nevertheless confident that the experimental method of investigating the equilibrium of forces and torques around drivers, as developed and applied in the present study, will prove useful in future investigations.

Acknowledgement

The authors thank Mr. Kenji Kawano and Mr. Hirofumi Kondo (Toyota Boshoku Corp.) for their collaboration.

References

(1) Yokoyama, S., Tanida, K. and Hashimoto, K., "The Method of Evaluating Muscle Strain while Maintaining Sitting Posture during Cornering and Strain Reduction by Seat Improvement", *JSAE Trans.* (in Japanese), Vol. 39, No. 4 (2008), pp. 177-182.
(2) Yamaguchi, T., Yamada, D. and Hada, M., "Effects of Pushing Steering Wheel and Shoulder Support on Mechanical Characteristics of Seat-driver-steering System", *AVEC'14* (2014), Article No. MoC3-4.
(3) Tomiyama, M., Kaneko, T., Osakabe, T., Hada, M. and Yasuda, E., "An Influence Analysis of Seat Performance on Vehicle Controllability", *Proc. JSAE* (in Japanese), No. 144-11 (2011), pp. 22-26.
(4) Hada, M, Yamaguchi, T., Goto, H., Kawano, K., Kimura, S., Kishi, S. and Shida, T., "An Analysis on Ease of Steer by Supporting Shoulder Girdle", *Proc. JSAE* (in Japanese), No. 6-12 (2012), pp. 15-20.
(5) Shimizu, N. and Imanishi, E., *Maruchibodei Dainamikusu 1* (in Japanese) (2006), pp. 60-76, *Coronasha*.
(6) Géradin, M. and Cardona, A., *Flexible Multibody Dynamics: A Finite Element Approach* (2001), pp. 58-61, John Wiley & Sons.
(7) Nobuhara, K., *Kata: Sono Kinou to Rinshou, Dai 3 pan* (in Japanese) (2004), 532p., *Igaku-Shoin*.

Takahiro Yamaguchi
Research Field:
- Physiological Science
Academic Degree: Dr.Sci.
Academic Societies:
- IEEE Engineering in Medicine and Biology Society
- Japanese Society for Medical and Biological Engineering
- Society of Automotive Engineers of Japan

Masatoshi Hada
Research Fields:
- Human Dynamics
- Biomechanics
- Ride Comfort of Vehicle
Academic Degree: Dr.Eng.
Academic Societies:
- Society of Automobile Engineers of Japan
- The Japan Society of Mechanical Engineers
- Society of Instrument and Control Engineers
Award:
- Tomoda Memorial Best Paper Award of SICE, 2008